Adaptation of a wood theoretical fracture model for predicting splitting capacity of dowelled connections in bamboo

Malkowska, D., Laux, T., Trujillo, D. & Norman, J.

Published PDF deposited in Coventry University's Repository

Original citation:
Malkowska, D, Laux, T, Trujillo, D & Norman, J 2022, 'Adaptation of a wood theoretical fracture model for predicting splitting capacity of dowelled connections in bamboo', Construction and Building Materials, vol. 357, 129358.
https://doi.org/10.1016/j.conbuildmat.2022.129358

DOI 10.1016/j.conbuildmat.2022.129358
ISSN 0950-0618
ESSN 1879-0526

Publisher: Elsevier

© 2022 The Authors. Published by Elsevier Ltd. This is an open access article under the CC BY license

Construction and Building Materials 357 (2022) 129358

Contents lists available at ScienceDirect

Construction and Building Materials

journal homepage: www.elsevier.com/locate/conbuildmat

Adaptation of a wood theoretical fracture model for predicting splitting capacity of dowelled connections in bamboo

Dominika Malkowska [a,*], Tobias Laux [b], David Trujillo [c], James Norman [d]

[a] University of Bristol, UK
[b] Bristol Composites Institute, University of Bristol, UK
[c] Coventry University, UK
[d] University of Bristol, UK

A B S T R A C T

A theoretical fracture model for predicting the splitting capacity of transversely loaded dowelled connections in timber was adapted to suit round bamboo. Existing experimental data obtained from a bespoke dowelled connection test for *G. angustifolia* (Guadua) bamboo was used to validate the model. It was found that the proposed theoretical model corresponds well with the experimental results. In addition, a simple numerical model was implemented using the Finite Element method to model the splitting capacity of the studied connection. The numerical results were found to correlate well with the experimental data. The study confirmed that the splitting capacity of transversely loaded dowelled connections in natural, unfilled bamboo internode can be effectively predicted with a theoretical timber fracture model as well as with the Finite Element analysis. The main outcome of the study is the characteristic equation for splitting capacity of a dowelled connection loaded perpendicular to fibre in round, unfilled Guadua bamboo.

1. Introduction

The world population reached 7.7 billion in 2019, and it is expected to reach 9.7 billion in 2050, with the largest increase due to happen in less developed and emerging economies [1]. Such a population increase will undoubtedly exert high demand on housing units worldwide, which amid the climate emergency ought to be alleviated sustainably, i.e., through efficient construction practices and the use of materials that are affordable, can be sourced locally and have the ability to store the atmospheric CO_2 [2]. An excellent example of such material is bamboo, which has been used as a construction material for centuries in many areas of the world due to its strength, availability, fast growth and low cost. Bamboo grows naturally in tropical and subtropical regions, the regions experiencing the most rapid population growth. It has been estimated that one billion people live currently in bamboo housing, most of them in traditional houses that use bamboo culms as their primary frame building material [3].

Bamboo is a giant grass native to all continents except Europe and Antarctica. The bamboo stem, called culm, is typically hollow, tapered and segmented. The segments are composed of internodes divided by interior diaphragms at nodes. The wall of the culm is composed of a hard, outer skin layer, a soft matrix material and the stronger uniaxial vascular bundles. The strength of the culm comes from the vascular bundles, similar to fibres in a fibre-reinforced matrix. Due to the fast rate of growth, it was shown that bamboo could potentially act as a very effective carbon sink, especially if regular and selective extraction is used [4].

Bamboo has been found to have excellent parallel-to-fibre properties, with some of the stronger bamboo species possessing similar strength properties to high-grade hardwood. This, however, is not the case for tension strength perpendicular to fibres which is much weaker than in timber due to the weak parenchyma matrix that holds the uniaxial fibres together [5]. The weak strength perpendicular to fibres together with the hollow and circular shape of bamboo leads to joints being one of the most difficult aspects to design. Therefore, although bamboo exhibits excellent tensile strength properties in the fibre axial direction, it is difficult to exploit its strength since the design is usually governed by the parenchyma matrix's weaknesses, i.e., shear strength when loaded parallel to fibres or tension strength perpendicular to fibres when loaded perpendicular to fibres. This characteristic significantly hinders bamboo connection design.

Despite the difficulties, several connection methods for bamboo culms have been developed, including mortise and tenon, lashed, clamped, and dowelled, among others [6]. Dowelled connections are one of the most widely used types of connections in bamboo construction. The connection is made with a steel bolt, and usually the bamboo internodes are filled with cement mortar (Fig. 1).

* Corresponding author.
E-mail addresses: dominika.malkowska@bristol.ac.uk (D. Malkowska), tobi.laux@bristol.ac.uk (T. Laux), david.trujillo@coventry.ac.uk (D. Trujillo), james.norman@bristol.ac.uk (J. Norman).

https://doi.org/10.1016/j.conbuildmat.2022.129358
Received 13 January 2022; Received in revised form 29 September 2022; Accepted 4 October 2022
Available online 10 October 2022
0950-0618/© 2022 The Authors. Published by Elsevier Ltd. This is an open access article under the CC BY license (http://creativecommons.org/licenses/by/4.0/).

Nomenclature

b	beam width
d	dowel diameter
f_c	compression strength parallel to fibres
$f_{t,90}$	tension strength perpendicular to fibres
f_v	shear strength parallel to fibres
h	beam height
h_e	distance from the loaded beam edge to the furthest fastener
k	shear coefficient
t	bamboo wall thickness
u	deflection
A	area
C_θ	factor accounting for the loading angle
D	external culm diameter
E	elastic modulus
E_c	energy of crack propagation
F	splitting capacity
G	shear modulus
G_f	fracture energy
G_{IC}, G_{IIC}, G_{IIIC}	critical fracture energy in mode I, II and III, respectively
$\sqrt{GG_f}$	fracture parameter
I	second moment of area
L	length of the specimen or span
M	bending moment
MC	moisture content
N	normal force
U	strain energy
V	shear force
W	work applied by external forces
α	factor of beam height
β	factor of crack propagation
θ	beam rotation OR angle between load and fibre direction
λ	length of crack propagation
μ	friction coefficient between steel and bamboo
ν	Poisson's ratio

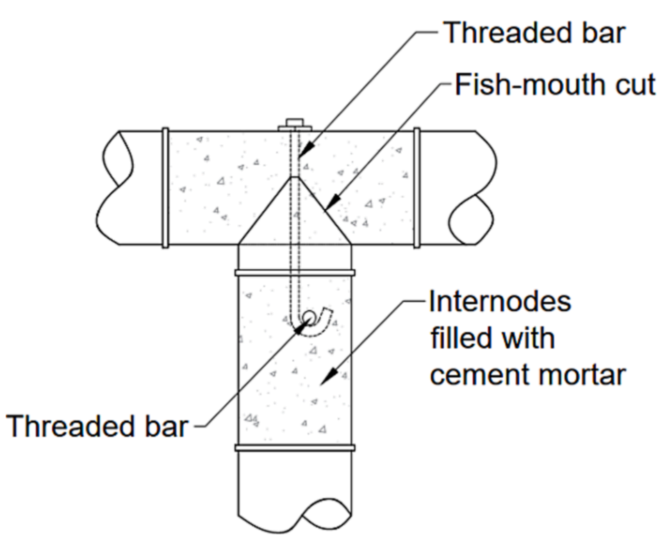

Fig. 1. Typical dowelled connection in bamboo construction.

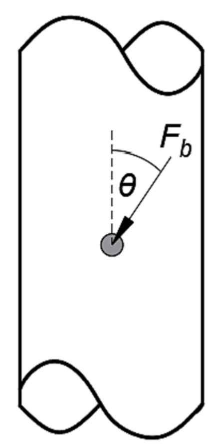

Fig. 2. Dowelled connection as in ISO 22156:2021 [7].

The available design guidance for dowelled connections in bamboo, as for any other structural aspect, is somewhat limited. Even though several structural design codes were developed, they provide limited guidance, especially in terms of the behaviour of connections. An exception to this is the recently published ISO 22156:2021 [7], which is arguably the most comprehensive design code for bamboo. The standard provides equations based on allowable stress design for the principle structural members, as well as for connections. The allowable bearing capacity (Fig. 2) F_b of a single dowel penetrating a single bamboo wall according to the standard is given as:

$$F_b = dtf_cC_\theta \tag{1}$$

where, for symmetrically loaded dowel engaging both culm walls: $C_\theta = 0.7$ if $0^\circ < \theta \leq 5^\circ$ and $C_\theta = 0.4$ if $\theta > 5^\circ$, d is dowel diameter, t is bamboo wall thickness, and f_c is bamboo compression strength parallel to fibres.

Eq. (1) is based on compression strength and contains the factor C_θ to take into account experimentally observed variations to embedment strength under various load angles. The standard provides splitting and shear equations that must be satisfied along with Eq. (1), however they only apply to joints with dowels loaded at $\theta \leq 5^\circ$. Prediction of splitting capacity for dowels loaded perpendicular to the fibres is therefore not explicitly considered. However, the design for splitting is covered by the requirement that connections transmitting shear force should be designed such that the least capacity of the connection is bearing failure under the dowel, which can be calculated with Eq. (1).

Apart from ISO 22156:2021 [7], another source of information, although more limited, is the Colombian Building Code NSR-10 [8], which provides allowable capacities for dowelled connections in internodes filled with cement mortar. The reported values are given in a tabular form for three bolt diameters (9.5, 12.7 and 15.9 mm) and only apply to connections made using Guadua. The reported capacities are based on compression and shear strength parallel to the fibres [9].

Predictive models for dowelled bamboo connections are sparse. Correal et al. [9] developed an analytical model to predict the yield strength of bamboo-to-bamboo dowelled connections filled with cement-mortar and loaded at various angles including parallel and perpendicular to fibres. The proposed model is a modified European Yield Model, which requires input in terms of geometrical properties of the connection, yield capacity of the dowel and bearing strengths of bamboo and mortar. The model was found to correlate well with the experimental results and the values contained in NSR-10 [8].

Most of the studies of dowelled bamboo connections focus on yield strength, assuming it being the critical failure mode of the connection.

Yielding, being ductile, is a desirable failure mode and provided that splitting is mitigated, dowelled connection capacity can be safely based on the yield strength prediction. However, the tendency of bamboo to split is a major weakness, and it must be understood in order to develop dowelled connection design guidelines with confidence.

To this end, this study aims to propose a theoretical model to predict the splitting capacity of transversely loaded dowelled connections in round, hollow (i.e., without mortar infill) bamboo. The derived model takes the form of a simple equation predicting the maximum splitting force in such connections. The model was validated against experimental results available in literature for Guadua, and therefore is only applicable to this species.

2. Theory

2.1. Eurocode 5 model

The proposed model for bamboo is based on the model derived for timber originally proposed by Gustafsson [10], and later expanded by Van Der Put and Leijten [11], which finally led to it being adopted in the current Eurocode 5 (EC5) [12] to estimate splitting capacity of dowelled connections in timber as:

$$F_{90,Rk} = 14b\sqrt{\frac{h_e}{1-h_e/h}} \tag{2}$$

$$F_{90,Rd} \geq F_{v,Ed}$$

$$F_{v,Ed} = max\{F_{v,Ed,1}, F_{v,Ed,2}\}$$

where $F_{v,Ed,1}, F_{v,Ed,2}$ are the design shear forces at either connection side as shown in Fig. 3.

The derivation of the splitting capacity is based on the assumption of a dowelled connection loaded perpendicular to the grain direction at the midspan of a simply supported beam (Fig. 4). The failure is caused by fracture at the connection in the beam midspan, where maximum bending stresses coincide with constant shear.

Van Der Put and Leijten [11] used the linear elastic beam theory to estimate maximum shear force V through determination of beam deflection u caused by crack propagation λ. The model assumes a simply supported beam of length $2L$, loaded by shear force $2V$ at the midspan (Fig. 5). When the beam separates into two parts, following a stable crack due to the shear force, the crack propagation has a length of λ, which has been assumed to be a function of the beam height h: $\lambda = \beta h$. The lower beam (beam 1) has height h_e, which also has been assumed to be a function of the beam height h: $h_e = \alpha h$. The lower beam (beam 1) is now loaded by bending moment M_1, shear force V and normal force N, whereas the upper beam (beam 2) is loaded by bending moment M_2 and

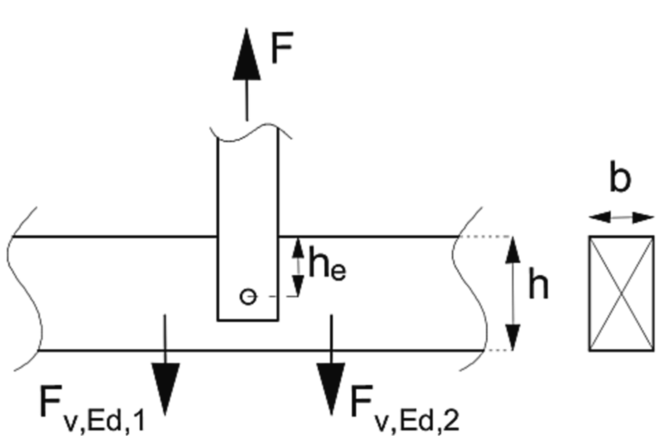

Fig. 3. Connection loaded perpendicular to grain (EC5).

normal force N.

The full derivations are shown in the Appendix.

The derived splitting capacity takes the form of:

$$V = b\sqrt{\frac{GG_f h\alpha^3}{0.6\alpha^2(1-\alpha)+1.5\beta^2 G/E}} \tag{3}$$

The derived formula (Eq. (3)) is a function of the crack length β, i.e. an initial fissure is assumed to exist in the beam. Van Der Put [34] demonstrated, that for small initial fissures, the term containing β can be ignored, hence the splitting capacity can be expressed as:

$$V = b\sqrt{\frac{GG_f h\alpha^3}{0.6\alpha^2(1-\alpha)}} \tag{4}$$

Van Der Put [34] further demonstrates that Eq. (4) can be applied to the design of uncracked dowelled connections. Finally, by substituting $\alpha h = h_e$ the final equation is obtained:

$$V = F_{90} = \sqrt{\frac{GG_f}{0.6}}b\sqrt{\frac{h_e}{1-h_e/h}} \tag{5}$$

The term $\sqrt{GG_f}$ was subsequently obtained from published data on dowelled tests in timber. Leijten and Van Der Put [13] divided the data into four categories (Fig. 6):

A – Over-designed connection, high value of $\sqrt{GG_f}$ as crack initiation stresses are developing over the whole cross-section depth.

B – Optimal designed connection, connection strength equals the splitting strength.

C – Under-designed connection, splitting failure after considerable slip, splitting is not the primary failure mode, low value of $\sqrt{GG_f}$.

D – Under-designed connection, splitting will not occur.

Crack growth is different for slender and stiff fasteners. The latter can be assigned to any of the A-D types. Type C for stiff fasteners is caused by exceeded embedment strength which allows for plastic movement of the fastener through the cross-section. Slender fasteners may bend, and therefore the crack gradually develops both along the grain and through the cross-section depth. These differences result in different values of $\sqrt{GG_f}$.

Based on the experimental results, it was proposed that $\sqrt{GG_f} = 12$ N/mm$^{3/2}$ [11], which is the lower bound since it corresponds to the connection type C. The upper limit, which corresponds to the over-designed connection (type A) was reported to be $\sqrt{GG_f} = 18.5$ N/mm$^{3/2}$ [11].

Therefore, the mean equation for the splitting capacity $F_{90,m}$ takes the form of:

$$F_{90,m} = \frac{12}{\sqrt{0.6}}b\sqrt{\frac{h_e}{1-h_e/h}} \tag{6}$$

2.2. Fracture theory

The fracture can be characterised by three different modes of failure (Fig. 7) or their combination. Mode I is caused by tension, mode II by shear and mode III by torsion. Structural components are subjected mostly to mixed mode I and II fracture, whereas mode III is rarely seen in practice.

The fracture energy G_f in the parameter $\sqrt{GG_f}$ represents a combination of modes I and II since the cross section at the dowel location is subjected to both tensile and shear stresses.

The majority of experimental studies of bamboo fracture energy were conducted using Moso. Shao et al. [14] tested Moso bamboo in a double cantilever bending configuration and reported values of $G_{IC} =$

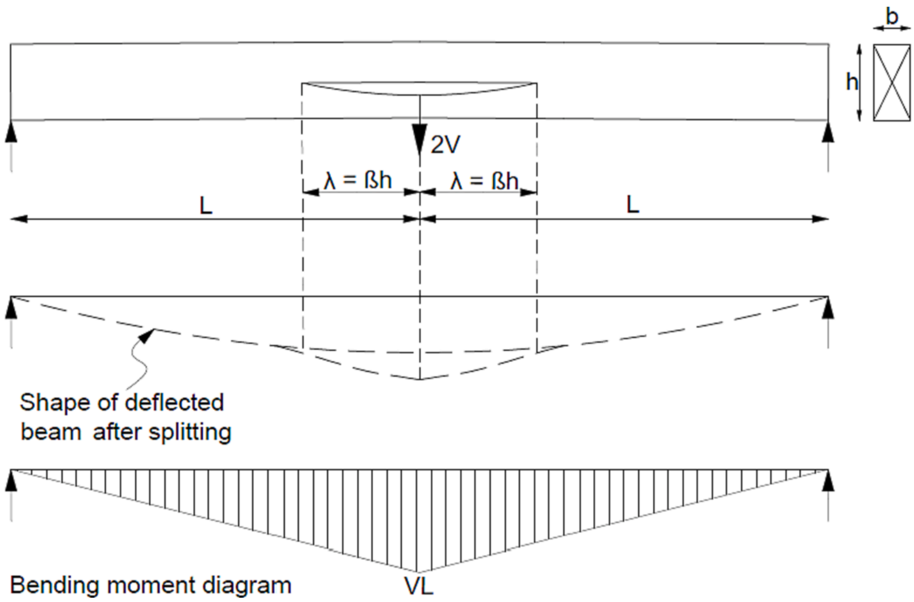

Fig. 4. Schematics of the beam (adapted from [11]).

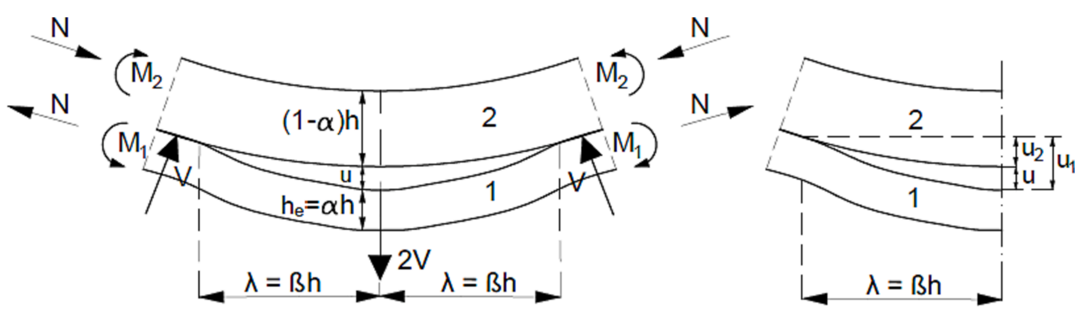

Fig. 5. Free body diagram in the cracked state (adapted from Van Der Put and Leijten [11]).

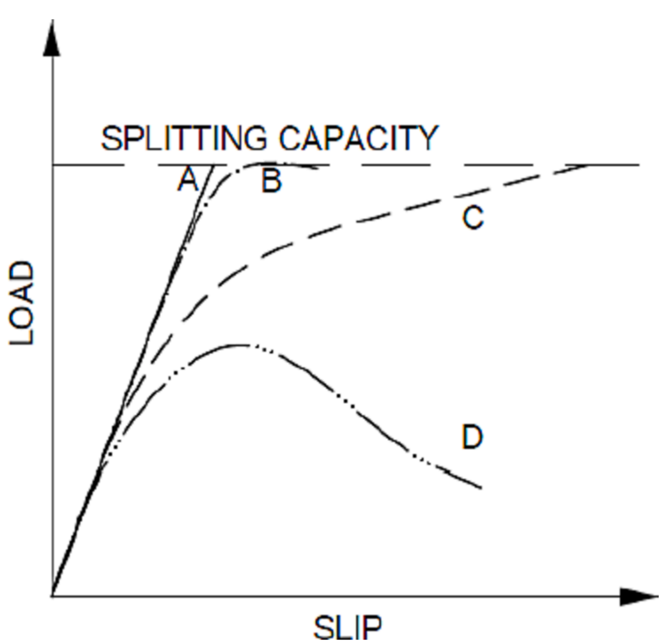

Fig. 6. Connection types with regard to load-slip behaviour (adapted from [13]).

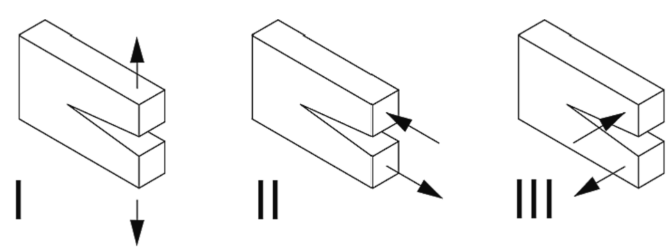

Fig. 7. Fracture modes: I opening, II shearing, and III tearing mode.

360 J/m^2. Tan et al. [15] tested Moso in a 4-point bending configuration with a notch in the mid-span, and reported values of G_{IC} = 800–6000 J/m^2 depending on where the notch was initiated (outside or inside culm surface). Wang et al. [16] tested Moso in mode II single end notched bending configuration and reported that G_{IIC} = 1300 J/m^2. Also Wang et al. [17] investigated the influence of nodes on fracture toughness using Moso in double cantilever bending test. The reported values were: $G_{IC,internode}$ = 500 J/m^2 and $G_{IC,node}$ = 1430 J/m^2. Mannan et al. [18] tested Male bamboo in double cantilever bending configuration and reported average G_{IC} of 750 J/m^2. Finally, Chen et al. [19] tested Moso in double cantilever bending configuration and reported values of G_{IC} starting from about 500 J/m^2 and increasing along with the crack length. However, the tested direction was radial-longitudinal, and not tangential-longitudinal, which is the typical crack direction in bamboo.

3. Derivation of model for bamboo

To adapt Eq. (6) to suit round bamboo, the following must be addressed:

1) Stiffness of the cross-section.
2) Shear coefficient.
3) The fracture parameter. $\sqrt{GG_f}$

3.1. Stiffness of bamboo cross-section

Bamboo has a hollow, cylindrical cross-section. The second moment of area I depends on the value of α (position of the dowel along the beam height), since the cross sections of the upper and lower beams can take different forms as shown in Fig. 8. Therefore, the second moment of area for the upper and lower beam was calculated separately for the case of $\alpha < 0.5$ and $\alpha > 0.5$ with the compound section method using equations available in the literature for the circle and the circle sector.

3.2. Shear coefficient for bamboo cross-section

The shear coefficient k must be evaluated for a hollow circular cross-section (uncracked state), as well as for cross-sections shown in Fig. 8 (cracked state). For a circular, hollow section, the shear coefficient was proposed, among others, by Armenakas et al. [20] as a function of Poisson's ratio ν:

$$k = \frac{1+\nu}{2+\nu} \tag{7}$$

The above formula assumes the walls are thin, meaning the shear stress is equal across the wall thickness. A formula for a hollow tube with an arbitrary thick wall (e.g. bamboo culm) was proposed by Stephen [21] as a function of Poisson's ratio ν and the inner to outer tube radius m:

$$k = \frac{6(1+\nu)^2(1+m^2)^2}{(7+34m^2+7m^4)+\nu(12+48m^2+12m^4)+\nu^2(4+16m^2+4m^4)} \tag{8}$$

For thin walls m tends to 1, and Eq. (8) becomes Eq. (7). Harries et al. [22] investigated D/t ratio of three common bamboo species: *B. stenostachya* (Tre Gai), *P. edulis* (Moso) and *G. angustifolia* (Guadua). It was concluded that the mean D/t values were 5.5 (Tre Gai), 10.3 (Moso) and 11.5 (Guadua), which translates to inner to outer radius ratio m of 0.64, 0.81, 0.83, respectively. Assuming the thickest cross-sections with ratio $m = 0.64$ (Tre Gai) and Poisson's ratio $\nu = 0.3$ in Eq. (8), the obtained shear factor k is 0.61, which is close to $k = 0.57$ obtained for infinitely thin cross-section (Eq. (7)). Therefore, for simplicity, the value of $k = 0.57$ was adopted in the derivations.

Considering the derivations above, the finally derived formula for bamboo F_{90} takes the form of:

$$F_{90} = \begin{cases} 2.67\sqrt{GG_f}\sqrt{\dfrac{t^2(D-t)(\pi+2asin(2\alpha-1))}{\pi-2asin(2\alpha-1)}}, & for\ \alpha \geq 0.5 \\ 2.67\sqrt{GG_f}\sqrt{\dfrac{t^2(D-t)(\pi-2asin(2\alpha-1))}{\pi+2asin(2\alpha-1)}}, & for\ \alpha \leq 0.5 \end{cases} \tag{9}$$

For $\alpha = 0.5$ the equations reduce to:

$$F_{90} = 2.67\sqrt{GG_f}\sqrt{t^2(D-t)} \tag{10}$$

Equation (10) is a general form equation for all hollow bamboo species.

3.3. The fracture parameter $\sqrt{GG_f}$ for Guadua bamboo

The derivation was followed by analysis of the existing experimental data for a bespoke dowelled connection test in Guadua [23].

3.3.1. Dowelled connection test methodology

The sample consisted of 62 dowelled connection tests, which were three-point bending tests with a dowelled connection at the midspan. Half of the sample consisted of specimens with the connection located in the mid-length of an internode (set A) and the other half of specimens with the connection near a node (set B). The testing set-up is shown in Fig. 9. A smooth 12 mm diameter steel pin was inserted through a pre-drilled hole at the specimen midspan to imitate a bolt connection. The beams were attached to a steel I-beam with a pair of metal straps positioned 60 mm away from beam ends. The pin was set to move upwards at a constant rate of 1 mm/min. In the specimens with the connection near node, the pin was inserted 25 mm away from the node. Density of the sample was not reported. The summary of the test configurations is shown in Table 1.

3.3.2. Dowelled connection test results

Based on the load–displacement graphs (Fig. 10), it was observed that most of the specimens appear to exhibit nearly linear-elastic behaviour until cracking occurred. It should be noted however, that the displacement data originates from the testing machine (cross-head displacement) and therefore may be subject to elastic deformation of the test set-up, specimen ovalisation and fibre crushing under the pin, in addition to deflection of the culm as beam. Consequently, the analysis of stiffness is excluded from the study, as it cannot be verified.

Typically, the crack propagation began at or near maximum load, which only in some cases led to complete failure. The lack of complete failure may be caused by the toughening impact of nodes, since as the crack opens, the distance to nodes decreases. The nodes have been previously shown to contribute to fracture toughness in bamboo [17]. In some cases, the cracking had begun before the maximum load was reached. In all cases the maximum load was read as F_{max}.

Examples of failure modes are shown in Fig. 11, where it can be noted that in the specimen with the connection near node, the crack length passing through the node is visibly shorter than on the other side

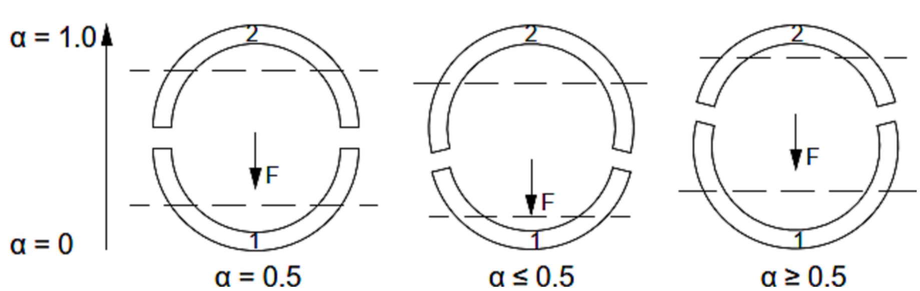

Fig. 8. Bamboo culm possible cross-sections after cracking depending on the initial dowel location along beam height, F – load direction, dashed line – axis for the second moment of area.

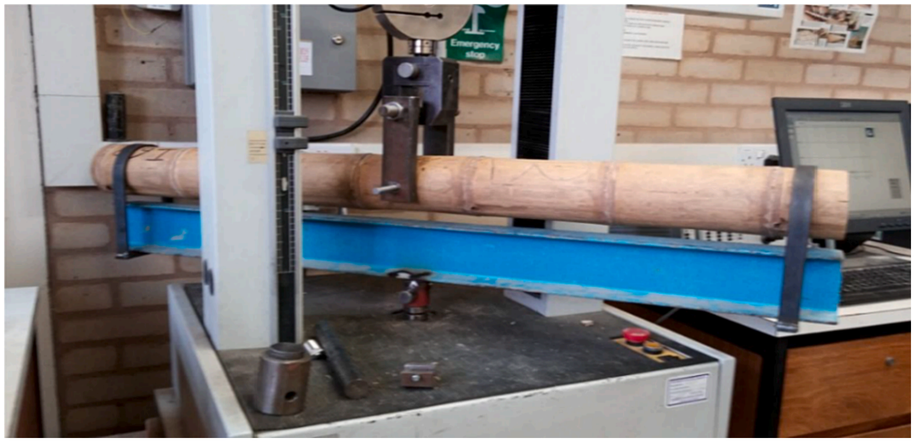

Fig. 9. Example of the connection test set-up for set A [23].

Table 1
Summary of the connection test configurations.

Span (between the straps) [mm]	Number of specimens (set A)	Number of specimens (set B)	Wall thickness *t* [mm]	Culm diameter *D* [mm]	MC [%]
300	1	–	5–19	62–118	10.2 CoV = 9.8 %
500	15	15			
750	15	16			
Total =	31	31			

of the pin, highlighting the node impact in hindering the crack propagation.

The fracture parameter $\sqrt{GG_f}$ was calculated separately for the sets A and B based on Eqs. (11)–(12). The summary of the test results is shown in Table 2.

$$\sqrt{GG_f} = \frac{F_{90}}{2.67\sqrt{t^2(D-t)}} \tag{11}$$

$$F_{max} = 2F_{90} \tag{12}$$

As anticipated, the mean value of $\sqrt{GG_f}$ was found to be higher for tests with the connection near node (set B) by approximately 17 % (Table 2). The span length was found to be irrelevant, which is in conformity with fracture theory.

The value of $\sqrt{GG_f} = 12.45$ N/mm$^{3/2}$ (set A) was applied in Eq. (10) to derive the final expression for the mean value of F_{90} [N], where D and t have units of mm:

$$F_{90} = 33.24\sqrt{t^2(D-t)} \tag{13}$$

Eq. (13) represents the mean value. To adapt it for design purposes, the characteristic equation, similar to Eq. (2), was derived using the 5-th percentile obtained through ranking of the experimental fracture parameter values $\sqrt{GG_f}_{0.05} = 9.79$ N/mm$^{3/2}$:

$$F_{90,k} = 26.14\sqrt{t^2(D-t)} \tag{14}$$

where $F_{90,k}$[N] is the force at either side of the connection, D is external diameter [mm] and t is wall thickness [mm].

The above equation is valid for any joint configuration, as long as the connector located furthest from the loaded edge is in the mid-height of the beam ($\alpha = 0.5$) and no yielding is observed before brittle failure (response type A in Fig. 6). Since only the configuration with a dowel at the beam mid-height was tested, Eq. (10) could not be validated for values other than $\alpha = 0.5$. However, in practice it is unlikely that a dowel will ever be placed anywhere different to mid-height. The fracture parameter $\sqrt{GG_f}$ was obtained from tests using only one dowel diameter size – 12 mm. According to the fracture theory, the obtained parameter value should be independent of the dowel diameter. However, fasteners with smaller diameters may yield before the brittle failure (response type C in Fig. 6), which may reduce the value of $\sqrt{GG_f}$. Additional testing using different dowel diameters would be required to prove this theory.

The derived mean equation (Eq. (13)) was plotted against the

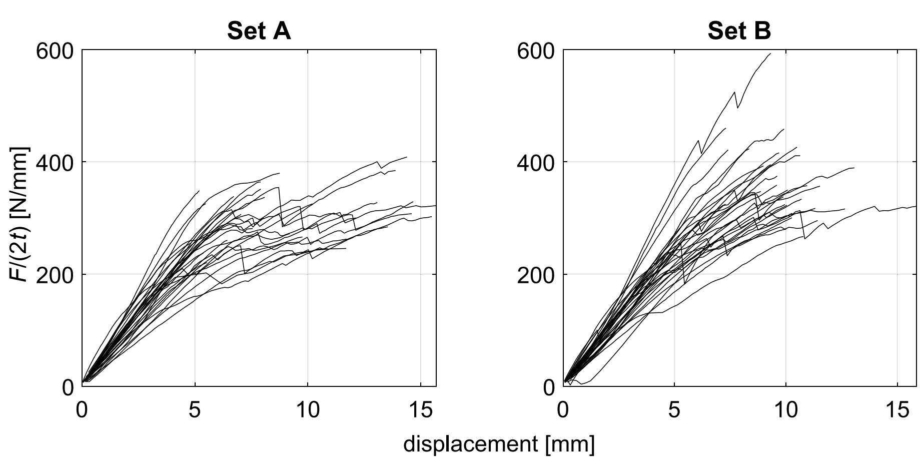

Fig. 10. Connection test – load adjusted for wall thickness plotted against displacement.

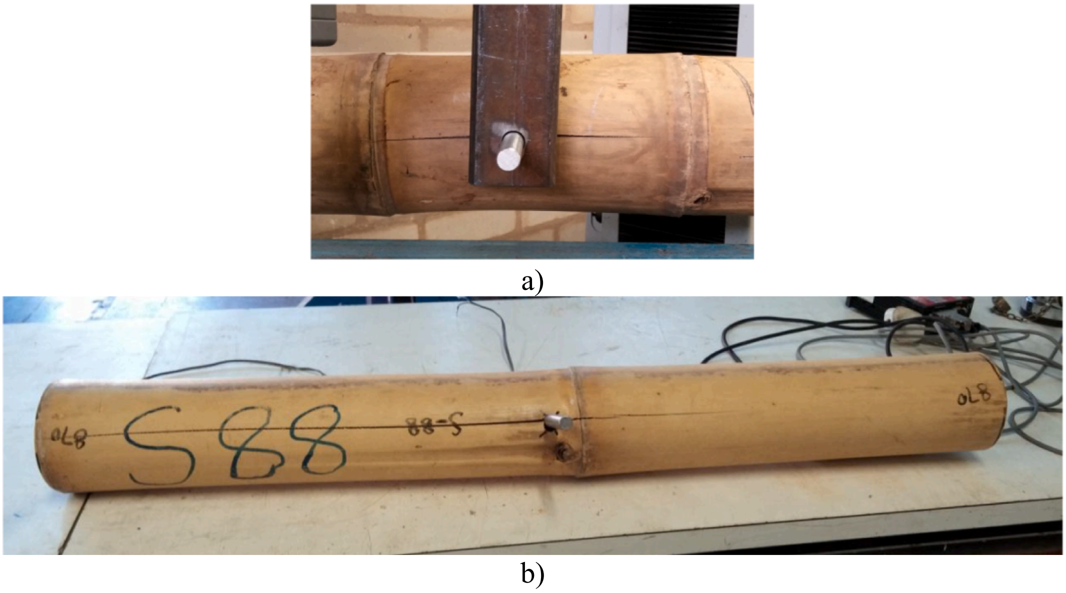

Fig. 11. Connection test – example of specimens after test: a) set A, b) set B (Li [23]).

Table 2
Summary of the connection test results.

	F_{max} [kN]	$\sqrt{GG_f}$ [N/mm$^{3/2}$]	$\sqrt{GG_f}$ (B) / $\sqrt{GG_f}$ (A)
set A	2.9–14.3	12.45 CoV = 17.5 %	14.51 / 12.45 = 1.17
set B	4.1–14.8	14.51 CoV = 19.9 %	

experimental data in Fig. 12. Since the derived equation is partially based on experimental results, the correlation between the prediction and the experimental results is expected. A better indication of the prediction goodness is the coefficient of variation, which as shown in Table 2, is below 20 % which is expected for a natural material like bamboo.

The parameter $\sqrt{GG_f}$ can also be directly calculated using the values of the shear modulus G and the fracture energy G_f. The value of the shear modulus G is assumed to be 580 N/mm^2 [24]. In the model derived for timber [11], the fracture energy G_f is assumed to be equal to the $G_{I,}$ fracture energy, as this is the dominant crack opening mode in case of the dowelled beam connection (compare Fig. 5 and Fig. 7). Due to the lack of reported values for Guadua, G_I is set to 0.6 N/mm, based on the reported range for Moso and Black bamboo of 0.36–0.8 N/mm ([14,15,18,19,25]).

Using the assumed values form literature, $\sqrt{GG_f}$ is calculated as 18.65 N/mm$^{3/2}$, which is comparable to the empirically obtained $\sqrt{GG_f}$ of 12.45 N/mm$^{3/2}$ for bamboo (see Table 2), and for timber (12–18 N/mm$^{3/2}$ [11]). The similarity between the calculated and the experimentally derived $\sqrt{GG_f}$ provides further confidence in the predictive capability and general applicability of the derived analytical formula in Eq. (10).

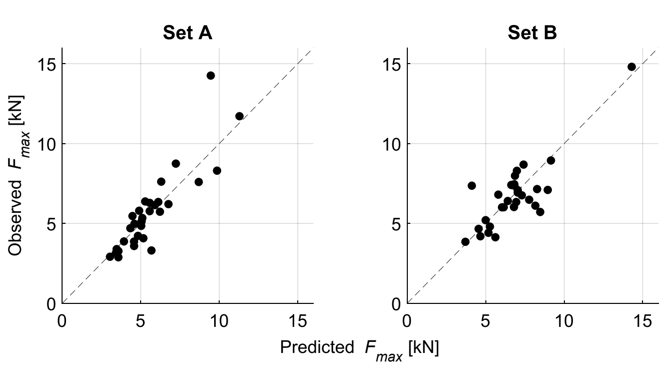

Fig. 12. Plots of predicted and observed splitting capacity.

4. Finite element analysis

The experimental tests of the dowelled connection at internode centre (set A in Fig. 10) was modelled using the commercial Finite Element (FE) software ABAQUS CAE/2018. To model the brittle crack initiation and propagation observed in the experiment, cohesive surfaces were placed parallel to the bamboo fibre direction at the expected crack planes (Fig. 13). This method is also used to model delamination between plies in multidirectional composite materials [26], where the surface of crack initiation and propagation is given by the microstructure of the material. This is also the case in bamboo, where cracks can be expected to propagate parallel to the fibre direction. A quasi-static explicit dynamic analysis was conducted to facilitate convergence due to the discretely nonlinear behaviour of the cohesive surfaces upon crack initiation [26].

To reduce the computational cost, a quarter model of the three-point bending experiment was constructed as shown in Fig. 13 by imposing symmetry boundary conditions on the longitudinal and transverse midplanes. The quarter model is simply supported on the right hand side, while a velocity boundary condition was imposed on the protruding external dowel surface. To meet the typical requirements for a quasi-static analysis, it was ensured that the kinetic energy does not exceed 5 % of the internal strain energy. A structured mesh aligned with the fibre direction of the bamboo was designed, and C3D8R brick elements with an approximate size of 1.5 mm in the refined area around the dowel were specified. Since the location of the crack initiation with respect to the dowel edge was not reported in the study by Li [23], it was decided to implement several cohesive surfaces distributed along the dowel edge along which the crack could propagate (Fig. 13). No plastic damage was specified in the model, since plasticity was not observed in the experimental tests. The bamboo material properties used in the model are contained in Table 3.

The steel dowel was modelled with elastic modulus of 210 GPa and Poisson's ratio 0.3. The stiffness constants (Table 3) of the bamboo were assigned using the transversely isotropic material model, with equal values in radial and transverse directions. The transverse isotropy was

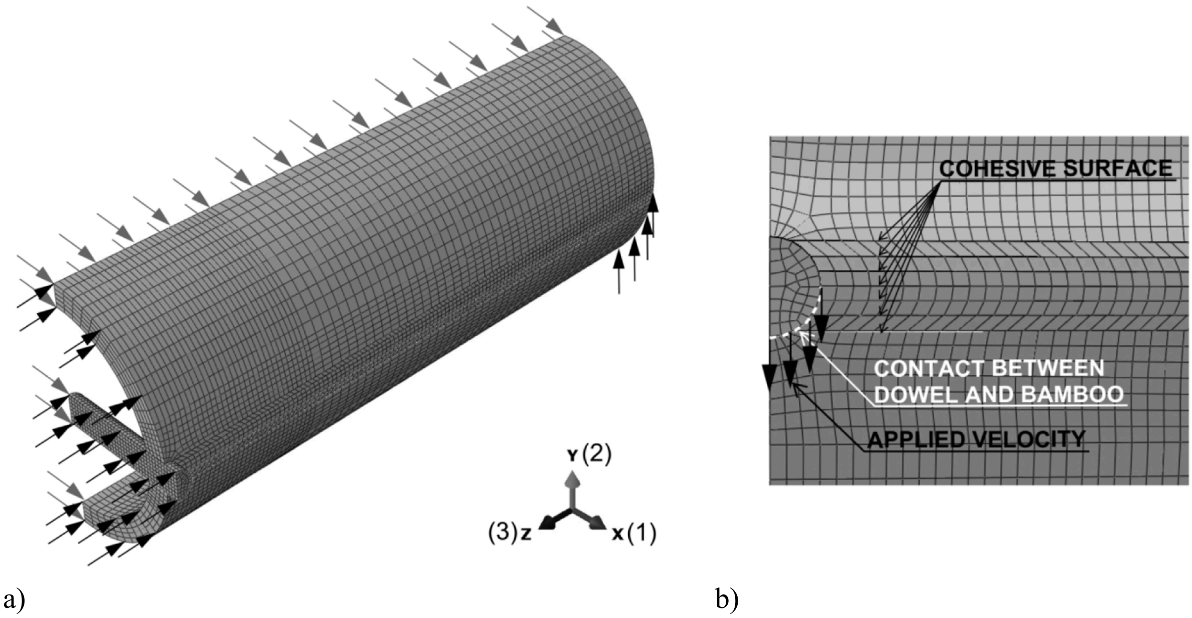

Fig. 13. a) Quarter model with the imposed boundary conditions, b) location of the imposed contact between dowel and bamboo and locations of the cohesive surfaces and applied velocity.

Table 3
Bamboo material properties. Subscripts 1, 2 and 3 denote radial, tangential and axial direction respectively.

	Material property	Unit	Value	Source / constitutive relation
Elastic constants	E_1	N/mm^2	400	[24]
	E_2	N/mm^2	400	$= E_1$
	E_3	N/mm^2	15,000	[27]
	ν_{12}	–	0.3	[24]
	ν_{13}	–	0.008	$= \nu_{32} E_1 / E_2$
	ν_{23}	–	0.008	$= \nu_{13}$
	ν_{32}	–	0.3	[27]
	G_{12}	N/mm^2	154	$= E_1 /(2 + 2\nu_{12})$
	G_{13}	N/mm^2	580	[24]
	G_{23}	N/mm^2	580	$= G_{13}$
Damage initiation	Normal stress, $f_{t,90}$	N/mm^2	1.3	[23]
	Shear stress in radial direction, f_{v1}	N/mm^2	7	[28]
	Shear stress in tangential direction, f_{v2}	N/mm^2	7	$= f_{v1}$
Damage evolution	Mode I fracture energy, G_{IC}	N/mm	0.6	[14,15,18,19,25]
	Mode II fracture energy, G_{IIC}	N/mm	1.8	$= 3G_{IC}$ [16]
	Mode III fracture energy, G_{IIIC}	N/mm	1.8	$= G_{IIC}$

previously used to model bamboo in a number of studies, e.g. Torres et al. [29], who concluded that a transversely isotropic model is able to capture the bamboo anisotropic features. The gradient of properties across bamboo wall thickness was not modelled, i.e. uniform properties were assigned in radial direction. The cohesive surface damage initiation criterion was based on the quadratic traction criterion expressed as:

$$\left(\frac{\sigma_n}{f_{t,90}}\right)^2 + \left(\frac{\tau_1}{f_{v1}}\right)^2 + \left(\frac{\tau_2}{f_{v2}}\right)^2 = 1 \quad (15)$$

where σ_n is nominal tangential stress; τ_1, τ_2 are nominal shear stresses in radial and axial direction, respectively; $f_{t,90}$ is tangential strength; and f_{v1} and f_{v2} are shear strength in radial and axial direction, respectively.

The mixed mode crack evolution was based on the Power Law energy criterion, with the exponent chosen as 1.0:

$$\left(\frac{G_I}{G_{IC}}\right)^1 + \left(\frac{G_{II}}{G_{IIC}}\right)^1 + \left(\frac{G_{III}}{G_{IIIC}}\right)^1 = 1 \quad (16)$$

where $G_{IC}, G_{IIC}, G_{IIIC}$ are the critical fracture energies required to cause failure in tangential, axial and radial direction, respectively, and where G_I, G_{II}, G_{III} represent the work done by the traction and its conjugate relative displacement in tangential, axial and radial direction, respectively.

Since it is anticipated that the splitting capacity is mostly dependent on the initiation stress and the propagation energy criteria, a sensitivity study was carried out to investigate the influence of those parameters. In addition, due to limited literature studies, the influence of the friction coefficient between steel dowel and bamboo was also investigated. The chosen parameters and their assumed values are shown in Table 4. The relations from Table 3 were used to estimate the values of f_{v2}, G_{IIC} and G_{IIIC}.

Due to the lack of published results of fracture energy for Guadua, the value for G_{IC} was judiciously chosen as 0.6 N/mm based on the sensitivity study and the reported range for Moso and Black bamboo of 0.36–0.8 N/mm ([14,15,18,19,25]), while G_{IIC} and G_{IIIC} were assumed to be equal to $3G_{IC}$ [16].

The contact behaviour between the steel dowel and the bamboo was modelled using the penalty stiffness method where the coefficient of friction between the steel dowel and bamboo was initially chosen as 0.4, which was followed by the sensitivity study (Table 4).

The initial analysis using several cohesive surfaces aimed to identify the location of the crack initiation with respect to the dowel edge. The analysis showed that the crack initiates at the surface located at dowel mid-height, although as analysis progresses another crack opens at a surface located below, near the first crack tip. With the confirmed

Table 4
Summary of the parameters used in the sensitivity study.

Analysis No	Investigated parameter	Friction coefficient, μ [-]	Normal stress, $f_{t,90}$ [N/mm^2]	Shear stress, f_v [N/mm^2]	Mode I fracture energy, G_{IC} [N/mm]
1 (default)	–	0.4	1.3	7	0.6
2	μ	**0.1**	1.3	7	0.6
3	μ	**0.8**	1.3	7	0.6
4	$f_{t,90}$	0.4	**0.5**	7	0.6
5	$f_{t,90}$	0.4	**2.5**	7	0.6
6	$f_{t,90}$	0.4	**15**	7	0.6
7	f_{v1}	0.4	1.3	**4**	0.6
8	f_{v1}	0.4	1.3	**10**	0.6
9	G_{IC}	0.4	1.3	7	**0.3**
10	G_{IC}	0.4	1.3	7	**0.9**

location of the first crack initiation, it was decided for the subsequent analysis to model the specimen with only one cohesive surface, as the aim of the model is to predict the peak load and not the complete damage evolution. The modelled specimen after failure is shown in Fig. 14.

The results from the sensitivity study are plotted against experimental data in Fig. 15. Overall, the assumed parameters appear to give a good prediction of the experimentally obtained splitting capacity. Stiffness was not modelled since as discussed, the experimental deflection was obtained directly from the test machine. The coefficient of friction between dowel and bamboo as well as the initiation shear stress f_{v1} have been found to have no impact on the capacity. The lack of influence of the shear stress f_{v1} could be explained by the boundary conditions at the crack initiation, that imply the shear stress at the crack surface will be zero due to the stress tensor symmetry. It should be noted however, that shear stress due to friction between the dowel and the hole is present at the hole to crack interface. This is however a localised stress, and as shown in the sensitivity study it does not affect the capacity.

The initiation tensile stress $f_{t,90}$ appears to affect the results to some extent, whereas mode I fracture energy G_{IC} has the biggest impact, which shows that the fracture energy is the most important parameter in the analysis of the splitting capacity. The studied range of $G_{IC} = 0.3$ – 0.9 N/mm appears to be appropriate for modelling Guadua although the values follow from studies on Moso and Black bamboo. Experimental study of fracture energy of Guadua is recommended to verify this assumption.

Very good match between the FE modelled capacity using default parameters (Table 4) and the analytical model prediction (Eq. (13)) was found, with the FE capacity being higher by 2.3 %. This finding indicates that the fracture parameter $\sqrt{GG_f}$ can be directly calculated from the FE splitting capacity using Eq. (11). The resulting value for the analysis with default parameters (Table 4) is $\sqrt{GG_f} = 12.65$ N/mm$^{3/2}$, which is close to the experimentally obtained value: $\sqrt{GG_f} = 12.45$ N/mm$^{3/2}$ (Table 2).

It should be noted that the theory presented in this study (see Section 2) leads to an analytical formula for predicting the splitting strength, whereas the FE model is a progressive failure analysis that predicts the full load response of the beam, i.e. the undamaged response, failure initiation, and damage progression. The crack onset (failure initiation) is modelled using a stress criterion, whereas the propagation criterion is based on fracture energy. The analytical model is simplistic as it does not replicate the full progressive failure progress as observed in the experiment and predicted by the FE model.

The FE cohesive zones model was chosen since in this approach no initial crack is required, which is a good representation of the modelled experiment with no pre-existing fissures. Also, the cohesive zone approach is well suited to study materials where the crack plane is known a priori, e.g. along the fibre direction, as it is in the case of bamboo, due to its low transverse strength in comparison to the high fibre longitudinal strength.

5. Conclusions

A simple equation based on fracture mechanics predicting maximum splitting capacity in dowelled, unfilled connections in bamboo was proposed. The derived equation contains a fracture parameter that needs to be assessed through experimental testing or through Finite Element analysis. The experimental tests and numerical analysis were carried out on Guadua bamboo.

The test results indicate that the connection response is stiff, and the critical failure is brittle. Brittle failure gives no warning before the structure collapses and should therefore be avoided. The studied connection had a simplistic design, which allowed for the verification of the theoretical derivations. It is anticipated that fasteners with smaller diameters would make the connection more ductile making it preferable over a single bolt.

The derived characteristic equation for Guadua is only valid for the range of tested configurations.

The Finite Element model was constructed using cohesive surfaces to model the brittle failure of the connection test. It was found that the splitting capacity is mostly affected by the mode I fracture energy. The assumed range of mode I fracture energy was based on values reported for Moso and Black bamboo, due to the lack of existing studies on Guadua.

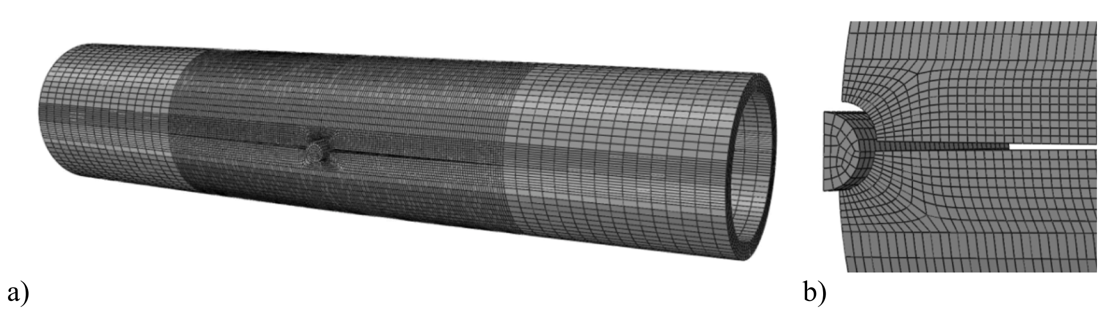

Fig. 14. a) Modelled specimen after failure, b) detailed view of the crack initiation.

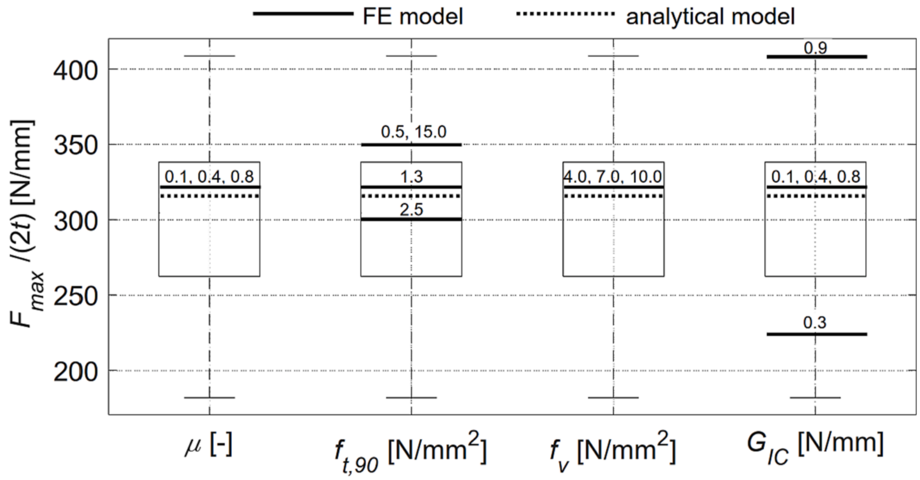

Fig. 15. Sensitivity study on the impact of μ, f_v, $f_{t,90}$ and G_{IC} on the modelled splitting capacity adjusted for wall thickness plotted against experimental data and the analytical model prediction (Eq. (13)).

Good correlation was found between the experimental data and the proposed analytical model, with coefficients of variation below 20 %, which is expected for a natural material like bamboo. The numerical model was found to correlate well with the analytical prediction and the experimental data, with the FE model resulting in approximately 2 % higher capacity than the analytical prediction.

The presented study provides an insight into the splitting capacity of transversely loaded dowelled bamboo connections. Even though, the clamps are often recommended to mitigate splitting in such connections, if ductility could be achieved through either yielding of the fastener(s) or fibre crushing under the fastener(s), the clamps potentially would not be necessary. Hence, the presented research could be used to further investigate the splitting capacity of connections with small-diameter fasteners, e.g. screws, which in theory, could lead to a ductile failure.

CRediT authorship contribution statement

Dominika Malkowska: Conceptualization, Methodology, Formal analysis, Software, Investigation, Validation, Investigation, Writing – original draft, Writing – review & editing. **Tobias Laux:** Software, Writing – review & editing. **David Trujillo:** Conceptualization, Methodology, Writing – review & editing. **James Norman:** Conceptualization, Methodology, Writing – review & editing, Funding acquisition.

Declaration of Competing Interest

The authors declare that they have no known competing financial interests or personal relationships that could have appeared to influence the work reported in this paper.

Data availability

Data will be made available on request.

Acknowledgement

The first author acknowledges the support of EPSRC (EP/R9004490).

Appendix

The model to predict the splitting capacity of timber is based on the Griffith Energy Balance, which states that the work applied by external forces W is equal the sum of the strain energy U and the energy of crack propagation E_c:

$$W = U + E_c \tag{A1}$$

For a simply supported beam loaded at the midspan by point load $2\ V$, it was shown that the deflection u is related to W and U as follows:

$$W = Vu \tag{A2}$$

$$U = Vu/2 \tag{A3}$$

From Eqs. (A.1)–(A.3) it follows that:

$$E_c = Vu/2 \tag{A4}$$

Since deflection u is related to V, the following can be assumed:

$$u = Vdu/dV \tag{A5}$$

For a constant value of V, Eq. (A.4) becomes:

$$E_c = V\frac{du}{dV}V/2 = \frac{V^2}{2}d(u/V) \tag{A6}$$

Energy of the crack extension can be also expressed as:

$$E_c = G_f A_c \tag{A7}$$

where A_c is the crack area:

$$A_c = bd(\beta h) \tag{A8}$$

and since h is constant:

$$A_c = bhd\beta \tag{A9}$$

Then Eq. (A.6) – (A.9) can be combined to:

$$V = \sqrt{\frac{2G_f\, bh}{\partial(u)/\partial(V\beta)}} \qquad \text{A 10}$$

The unknown terms in Eq. (A.10) are: $\partial(u)/\partial(V\beta)$ and fracture energy G_f. The fracture energy follows from experimental results . The first term denominates the change of cracking deflection u in relation to the increase of crack extension β for a constant V.

The cracking deflection u denominates the difference in deflection between cracked and uncracked state u_1 and u_2, respectively (Eq. A.11). Since the relative difference in deflection between upper and lower beam in the region beyond the crack (between crack tip and beam support) is zero, the deflection needs to be calculated only in the crack propagation area λ (Fig. 5).

$$u = u_1 - u_2 \qquad \text{A 11}$$

Following from the elastic beam theory for a beam cross-section with elastic modulus E, second moment of area I, and subjected to a bending moment as a function of the beam length $M(x)$, the bending deflection can be calculated at any point by integrating the function of beam rotation $\theta(x)$:

$$u_{bending}(x) = \int \theta(x)\, dx = \int\int \frac{M(x)}{EI(\alpha)}\, dx \qquad \text{A 12}$$

By accounting for compatibility between rotations at the crack tip of the upper and lower beam as well as compatibility between bending moments in cracked and uncracked state (details in [11]), the bending deflection increase due to cracking is calculated as:

$$u_{bending} = \frac{V\beta^3}{E\alpha^3 b} \qquad \text{A 13}$$

In addition to bending deflection, the contribution from shear deflection should be accounted for. The shear deflection can be calculated from the Timoshenko–Ehrenfest beam theory [30] as:

$$u_{shear}(x) = \int \frac{V}{kAG} dx \qquad \text{A 14}$$

The shear coefficient k accounts for the fact that the shear stress is not uniform over the cross section. There have been many attempts to evaluate the value of k theoretically and experimentally. According to Kaneko [31], the most accurate formula for rectangular beams is the equation suggested first by Timoshenko [32]:

$$k = \frac{5}{6+5\nu} + \frac{5\nu}{6+5\nu} \qquad \text{A 15}$$

Other researchers proposed different formulas, among them $k = 5/6$ by Goens [33]. The value of $k = 5/6 = 0.833$ is similar to the one proposed by Timoshenko for $\nu = 0.3$ ($k = 0.867$), and it appears to be commonly used in engineering practice. Implementing $k = 5/6$, the shear deflection increase due to cracking is:

$$u_{shear} = \frac{1.2V}{G}\left(\frac{\beta h}{b\alpha h} - \frac{\beta h}{bh}\right) \qquad \text{A 16}$$

Combining the bending and shear deflection gives:

$$u = \frac{V\beta^3}{E\alpha^3 b} + \frac{1.2V}{G}\left(\frac{\beta h}{b\alpha h} - \frac{\beta h}{bh}\right) \qquad \text{A 17}$$

The obtained formula for deflection can now be differentiated to obtain the term $\partial(u)/\partial(V\beta)$ needed in Eq. (A.10). For a constant value of V:

$$\partial(u)\Big/\partial(V\beta) = \frac{du}{d\beta}\frac{1}{V} \qquad \text{A 18}$$

Differentiating the equation above gives:

$$\frac{du}{d\beta} = \frac{3V\beta^2}{E\alpha^3 b} + \frac{1.2V}{G}\left(\frac{h}{b\alpha h} - \frac{h}{bh}\right) \qquad \text{A 19}$$

$$\partial(u)\Big/\partial(V\beta) = \frac{3\beta^2}{E\alpha^3 b} + \frac{1.2}{bG}\left(\frac{1}{\alpha} - 1\right) \qquad \text{A 20}$$

Inserting Eqs. (A.20) into Eq. (A.10) gives:

$$V = b\sqrt{\frac{GG_f\, h\alpha^3}{0.6\,\alpha^2(1-\alpha) + 1.5\beta^2 G/E}} \qquad \text{A 21}$$

Van Der Put [34] postulated, that the values of $1.5\beta^2 G/E$ in Eq. (A.21) were small, since by assuming $1.5\beta^2 G/E = 0$ the fit of the derived formula was as good as when $1.5\beta^2 G/E \neq 0$.

Therefore:

$$V = b\sqrt{\frac{GG_f\,h\,\alpha^3}{0.6\,\alpha^2(1-\alpha)}} \quad \text{A 22}$$

By substituting $\alpha h = h_e$ the final equation is obtained:

$$V = F_{90} = \sqrt{\frac{GG_f}{0.6}}\,b\,\sqrt{\frac{h_e}{1-h_e/h}} \quad \text{A 23}$$

References

[1] Department of Economic and Social Affairs. Population Division, "World Population Prospects: Highlights," United Nations, New York, 2019.
[2] G. Churkina, A. Organschi, C.P.O. Reyer, A. Ruff, K. Vinke, Z. Liu, B.K. Reck, T. E. Graedel, H.J. Schellnhuber, Buildings as a global carbon sink, Nat. Sustainability 3 (4) (2020) 269–276.
[3] Food and Agriculture Organisation of the United Nations FAO, "World Bamboo Resources. Non-Wood Forest Products," United Nations, Rome, 2007.
[4] L. Kuehl and K. Yiping, "Carbon Off-Setting with Bamboo," in *International Network for Bamboo and Rattan. INBAR*, Beijing, P.R. China, 2012.
[5] S. Kaminski, A. Lawrence, D. Trujillo, Structural use of bamboo: Part 1: Introduction to bamboo, Struct. Eng. 94 (8) (2016) 40–43.
[6] A. Widyowijatnoko, K.A. Harries, in: "Joints in Bamboo Construction", in *Nonconventional and vernacular construction materials*, Elsevier Woodhead Publishing, 2019, pp. 561–596.
[7] International Organization for Standardization, "Bamboo structures — Bamboo culms — Structural design (ISO 22156:2021)".
[8] Asociación Colombiana de Ingeniería Sísmica, Reglamento Colombiano de Construcción Sismo Resistente NSR-10, 2012.u.
[9] J.F. Correal, E. Prada, A. Suárez, D. Moreno, Bearing capacity of bolted-mortar infill connections in bamboo and yield model formulation, Constr. Build. Mater. 305 (2021) 124597.
[10] P. Gustafsson, "A study of strength of notched beams," in CIB W18 Timber Structures Proceedings, 21-10-1, 1988.
[11] T. Van Der Put and A. Leijten, "Evaluation of perpendicular to grain failure of beams caused by concentrated loads of joints," in CIB W18 Timber Structures Proceedings, 33-7-7, 2000.
[12] European Committee for Standardization, Eurocode 5: Design of Timber Structures, BSI, Brussels, 1994.
[13] A. Leijten T. Van Der Put Splitting strength of beams loaded perpendicular to grain by connections, a fracture mechanical approach 2004 Lahti, Finland.
[14] Z. Shao, C. Fang, G. Tian, Mode I interlaminar fracture property of Moso bamboo (Phyllostachys pubescens), Wood Sci. Technol. 43 (5–6) (2009) 527–536.
[15] T. Tan, N. Rahbar, S.M. Allameh, S. Kwofie, D. Dissmore, K. Ghavami, W. O. Soboyejo, Mechanical properties of functionally graded hierarchical bamboo structures, Acta Biomater. 7 (10) (2011) 3796–3803.
[16] F. Wang, Z. Shao, Y. Wu, Mode II interlaminar fracture properties of Moso bamboo, Compos. B Eng. 44 (1) (2013) 242–247.
[17] F. Wang, Z. Shao, Y. Wu, D. Wu, The toughness contribution of bamboo node to the Mode I interlaminar fracture toughness of bamboo, Wood Sci. Technol. 48 (6) (2013) 1257–1268.
[18] S. Mannan, V. Parameswaran, S. Basu, Stiffness and toughness gradation of bamboo from a damage tolerance perspective, Int. J. Solids Struct. 143 (2018) 274–286.
[19] Q. Chen, C. Dai, C. Fang, M. Chen, S. Zhang, R. Liu, X. Liu and B. Fei, Mode I interlaminar fracture toughness behaviour and mechanisms of bamboo, Materials Design, vol. 183, 2019.
[20] A. Armenakas, D. Gazis and G. Herrmann, Free Vibrations of Circular Cylindrical Shells, London: Pergamon Press.
[21] N. Stephen, Timoshenko's Shear Coefficient from a Beam Subjected to Gravity Loading, *J. Appl. Mech.,* 47 (1), 1980.
[22] K.A. Harries, J. Bumstead, M. Richard, D. Trujillo, Geometric and material effects on bamboo buckling behaviour, Proc. Inst. Civil Eng. – Struct. Build. 170 (4) (2017) 236–249.
[23] Y. Li, Splitting Failure of Bamboo Culms, Coventry University, UK, 2015 thesis.
[24] J. García, C. Rangel, K. Ghavami, Experiments with rings to determine the anisotropic elastic constants of bamboo, Constr. Build. Mater. 31 (2012) 52–57.
[25] F. Wang, Z. Shao, Y. Wu, D. Wu, The toughness contribution of bamboo node to the Mode I interlaminar fracture toughness of bamboo, Wood Sci. Technol. 48 (6) (2014) 1257–1268.
[26] T. Laux, K. Gan, R. Tavares, C. Furtado, A. Arteiro, P. Camanho, O. Thomsen, J. Dulieu-Barton, Modelling damage in multidirectional laminates subjected to multi-axial loading: Ply thickness effects and model assessment, Compos. Struct. 266 (2021).
[27] K. Ghavami and A. Marinho, "Propriedades físicas e mecânicas do colmo inteiro do bambu da espécie Guadua angustifolia," Revista Brasileira de Engenharia Agrícola e Ambiental, vol. 9(1), 2005.
[28] J. Correal, J. Arbeláez, Influence of age and height position on Colombian Guadua Angustifolia bamboo mechanical properties, Maderas, Ciencia y tecnología 12 (2) (2010) 105–111.
[29] L. Torres, K. Ghavami, J. Garcia, A transversely isotropic law for the determination of the circumferential Young's modulus of bamboo with diametric compression tests, Latin Am. Appl. Res. (2007).
[30] S. Timoshenko, On the correction for shear of the differential equation for transverse vibrations of prismatic bar, Phil. Mag. 41 (1921) 744–746.
[31] T. Kaneko, On Timoshenko's correction for shear in vibrating beams, J. Phys. D Appl. Phys. (1975).
[32] S. Timoshenko, On the transverse vibrations of bars of uniform crosssection, The London, Edinburgh, Dublin Philos. Mag. J. Sci. 43 (253) (1922) 125–131.
[33] E. Goens, Über die Bestimmung des Elastizitätsmoduls von Stäben mit Hilfe von Biegungsschwingungen, Ann. Phys. 11 (1931) 649–678.
[34] T. Van Der Put, A new fracture mechanics theory of wood. Extended Second Edition, New York: Nova Science Publishers, 2017.